Engineering Computations

A numerical investigation of transient MHD free convective flow of a nanofluid over a moving semi-infinite vertical cylinder

V. Rajesh, A.J. Chamkha, Ch. Sridevi, A.F. Al-Mudhaf,

A numerical investigation of transient MHD free convective flow of a nanofluid over a moving semi-infinite vertical cylinder

V. Rajesh
Department of Engineering Mathematics, GITAM University Hyderabad Campus, Hyderabad, India

A.J. Chamkha
Department of Manufacturing Engineering, Prince Mohammad Bin Fahd University, Al-Khobar, Saudi Arabia and Prince Sultan Endowment for Energy and Environment, Prince Mohammad Bin Fahd University, Al-Khobar, Saudi Arabia

Ch. Sridevi
Department of Mathematics, Vidya Jyothi Institute of Technology, Hyderabad, India, and

A.F. Al-Mudhaf
Manufacturing Engineering Department, The Public Authority for Applied Education, Shuwaikh, Kuwait

Received 19 March 2016
Revised 6 September 2016
20 October 2016
Accepted 25 October 2016

Abstract

Purpose – The purpose of this paper is to study numerically the influence of a magnetic field on the transient free convective boundary layer flow of a nanofluid over a moving semi-infinite vertical cylinder with heat transfer

Design/methodology/approach – The problem is governed by the coupled non-linear partial differential equations with appropriate boundary conditions. The fluid is a water-based nanofluid containing nanoparticles of copper. The Brinkman model for dynamic viscosity and Maxwell–Garnett model for thermal conductivity are used. The governing boundary layer equations are written according to The Tiwari–Das nanofluid model. A robust, well-tested, implicit finite difference method of Crank–Nicolson type, which is unconditionally stable and convergent, is used to find the numerical solutions of the problem. The velocity and temperature profiles are studied for significant physical parameters such as the magnetic parameter, nanoparticles volume fraction and the thermal Grashof number Gr. The local skin-friction coefficient and the Nusselt number are also analysed and presented graphically.

Findings – The present computations have shown that an increase in the values of either magnetic parameter M or nanoparticle volume fraction decreases the local skin-friction coefficient, whereas the opposite effect is observed for thermal Grashof number Gr. The local Nusselt number increases with a rise in Gr and ϕ values. But an increase in M reduces the local Nusselt number.

Originality/value – This paper is relatively original and presents numerical investigation of transient two-dimensional laminar boundary layer free convective flow of a nanofluid over a moving semi-infinite vertical cylinder in the presence of an applied magnetic field. The present study is of immediate application to all those processes which are highly affected by heat enhancement concept and a

Engineering Computations
Vol. 34 No. 5, 2017
pp. 1393-1412

0264-4401
DOI 10.1108/EC-03-2016-0090

magnetic field. Further the present study is relevant to nanofluid materials processing, chemical engineering coating operations exploiting nanomaterials and others.

Keywords MHD, Cu–water nanofluid, Free convection, Implicit finite difference numerical method, Transient flow, Vertical cylinder

Paper type Research paper

Nomenclature

Ag = silver;
Al_2O_3 = aluminium oxide;
C_f = skin friction coefficient;
C_p = specific heat at constant pressure (J kg^{-1} K^{-1});
Cu = copper;
g = acceleration due to the gravity (m s^{-2});
Gr = thermal Grashof number;
Nu_x = local Nusselt number;
Pr = Prandtl number;
r = radial coordinate normal to the cylinder (m);
r_0 = radius of the cylinder (m);
R = dimensionless radial coordinate normal to the cylinder;
t = dimensionless time;
T = dimensionless temperature;
t' = time (s);
T' = temperature of the fluid (K);
TiO_2 = titanium oxide;
T'_w = temperature of the cylinder;
T'_∞ = temperature of the fluid far away from the cylinder;
u = velocity component in the x-direction (m s^{-1});
U = dimensionless velocity component in the X-direction;
v = velocity component in the r-direction (m s^{-1});
V = dimensionless velocity component in the R-direction;
x = spatial coordinate along the cylinder (m);
X = dimensionless spatial coordinate along the cylinder;
β = volumetric thermal expansion coefficient (K^{-1});
Δt = grid size in the time;
ΔR = grid size in the radial direction;
ΔX = grid size in the axial direction;
κ = thermal conductivity (J m^{-1} K^{-1});
μ = dynamic viscosity (Pa s);
ν = kinematic viscosity (m^2 s^{-1});
ρ = density (kg m^{-3});
σ = electrical conductivity (S m^{-1}); and
ϕ = solid volume fraction of nanoparticles.

Subscripts

f = base fluid;
i = grid point along the X-direction;
j = grid point along the R-direction;

nf = nanofluids;
s = solid nanoparticles;
W = conditions on the wall; and
∞ = free stream condition.

Superscript

n = grid point along the t-direction.

1. Introduction

Transient natural convection flow of a viscous incompressible fluid over a heated vertical cylinder is an important problem relevant to many engineering applications. The boundary layer flow and heat transfer due to stretching flat plates or cylinders are of practical importance in glass and fibre technologies and extrusion processes. The production of polymer sheets and cylinders and plastic films is based on this technology. There are number of examples which include the cooling of an infinite metallic plate or hot filaments, which are considered as vertical cylinders, in a cooling bath, the boundary layer along material handling conveyers, the aerodynamic extrusion of plastic sheets or cylinders, the boundary layer along a liquid film in condensation processes, paper production, glass blowing, metal spinning and drawing plastic films and polymer extrusion. The quality of the final product depends on the rate of heat transfer at the stretching surface or cylinder. Using a nanofluid under special circumstances has proven to enhance the heat transfer, which in turn, enhances the quality of the final stretched surface or cylinder. Sparrow and Gregg (1956) studied the laminar buoyant flow of air bathing a vertical cylinder heated with a prescribed surface temperature. Chen and Yuh (1980) considered the effects of heat and mass transfer on natural convective flow along a vertical cylinder. The problem of natural convection in laminar boundary layer flow along slender vertical cylinders and needles is presented by Lee *et al.* (1988). Velusamy and Garg (1992) studied the transient natural convection over heat-generating vertical cylinder. Ganesan and Rani (1999) investigated unsteady natural convection flow along vertical cylinder with variable heat and mass transfer. Rani (2003) studied transient natural convection along a vertical cylinder with variable temperature and mass diffusion.

Transient MHD free convection flow due to impulsive motion of a solid body has a number of applications in engineering and technology. Seth and Ansari (2010) studied MHD natural convection flow past an impulsively moving vertical plate with ramped wall temperature in the presence of thermal diffusion with heat absorption. Seth *et al.* (2011a) investigated MHD natural convection flow with radiative heat transfer past an impulsively moving plate with ramped wall temperature. Seth *et al.* (2011b) studied the effect of rotation on unsteady hydromagnetic natural convection flow past an impulsively moving vertical plate with ramped temperature in a porous medium with thermal diffusion and heat absorption. Khedr *et al.* (2009) investigated MHD flow of a micropolar fluid past a stretched permeable surface with heat generation or absorption. Seth *et al.* (2013) analysed the effects of thermal radiation and rotation on unsteady hydromagnetic free convection flow past an impulsively moving vertical plate with ramped temperature in a porous medium. Nandkeolyar *et al.* (2013) studied unsteady hydromagnetic natural convection flow of a dusty fluid past an impulsively moving vertical plate with ramped temperature in the presence of thermal radiation. Seth *et al.* (2015a) investigated effects of hall current and rotation on hydromagnetic natural convection flow with heat and mass transfer of a heat-absorbing fluid past an impulsively moving vertical plate with ramped temperature. Seth and Sarkar (2015) studied MHD natural convection heat and mass transfer flow past a time-

dependent moving vertical plate with ramped temperature in a rotating medium with Hall effects, radiation and chemical reaction. Seth *et al.* (2015b) analysed unsteady hydromagnetic natural convection flow past an impulsively moving vertical plate with Newtonian heating in a rotating system. Moreover, Rashidi *et al.* (2014) studied mixed convective heat transfer for MHD viscoelastic fluid flow over a porous wedge with thermal radiation. Rashidi *et al.* (2012) presented analytic approximate solutions for MHD boundary layer viscoelastic fluid flow over continuously moving stretching surface by Homotopy analysis method with two auxiliary parameters. Rashidi and Erfani (2012) investigated analytical method for solving steady MHD convective and slip flow owing to a rotating disk with viscous dissipation and Ohmic heating.

On the other hand, due to the number of applications of nanofluids in many areas of engineering and technology, Loganathan *et al.* (2013) analytically studied the effects of radiation on an unsteady natural convective flow of a nanofluid past an impulsively started infinite vertical plate. Rajesh and Anwar Beg (2014) numerically analysed the effects of MHD on the transient free convection flow of a viscous, electrically conducting and incompressible nanofluid past a moving semi-infinite vertical cylinder with temperature oscillation. Abolbashari *et al.* (2014) studied Entropy analysis for an unsteady MHD flow past a stretching permeable surface in a nanofluid. Rajesh *et al.* (2015a) investigated the transient free convection flow and heat transfer of a viscous electrically conducting and incompressible nanofluid past a moving semi-infinite vertical plate subject to hydromagnetic, radiation and temperature oscillation effects. Later a mathematical model is developed for the nanofluid flow and heat transfer due to the impulsive motion of an infinite vertical porous plate in its own plane in the presence of a magnetic field and viscous dissipation by Rajesh *et al.* (2015b). Also, Rajesh *et al.* (2016a) presented a mathematical model for the unsteady free convective flow and heat transfer of a viscous nanofluid from a moving vertical cylinder in the presence of thermal radiation. Further Rajesh *et al.* (2016b) studied the influence of magnetic field on the nanofluid flow and heat transfer due to the impulsive motion of a semi-infinite vertical plate by the implicit finite difference numerical method. Recently, Rajesh *et al.* (2016c) presented a numerical study of transient natural convection flow of an incompressible viscous nanofluid and heat transfer from an impulsively started semi-infinite vertical plate with variable surface temperature.

The objective of this paper is therefore to study the influence of a magnetic field on the transient free convective boundary layer flow of a nanofluid past a moving semi-infinite vertical cylinder with heat transfer. A numerical solution by an implicit finite-difference method of the Crank–Nicolson type is obtained. The transient velocity and temperature profiles and the axial distributions of the skin-friction coefficient and local Nusselt number are presented graphically and discussed. The present study is of immediate application to all those processes which are highly affected by heat enhancement concept and a magnetic field.

2. Mathematical model

The transient laminar two-dimensional boundary layer free convective flow of a viscous incompressible electrically conducting nanofluid past a moving semi-infinite vertical cylinder of radius r_0 in the presence of an applied magnetic field is considered. The x-axis is taken along the axis of the cylinder in the vertically upward direction and the radial coordinate r is taken normal to the cylinder as shown in Figure 1. The gravitational acceleration g acts downward. Initially, both the cylinder and the nanofluid are stationary and at the same temperature T'_∞. They are maintained at this condition for all $t' \leq 0$. At time $t' > 0$, the cylinder starts moving in the vertical direction with a uniform velocity u_0. The temperature on the surface of the cylinder is raised to T'_w and is maintained at the same value. We assume that the uniform magnetic field with intensity of B_0 acts in the radial direction and the effects of the induced magnetic field

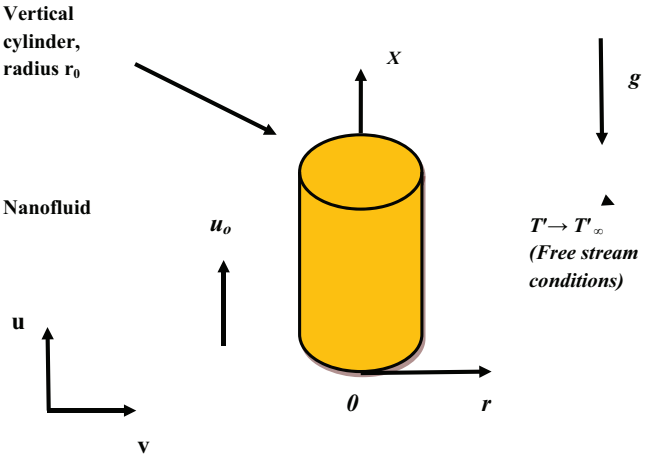

Figure 1.
The physical model and coordinate system

are negligible, which is valid when the magnetic Reynolds number is small. The viscous dissipation, Ohmic heating and the Hall effects are neglected, as they are also assumed to be small. The fluid is a water-based nanofluid containing copper (*Cu*) nanoparticles. In this study, the nanofluid is assumed to behave as a single-phase fluid with local thermal equilibrium between the base fluid and the nanoparticles suspended in it so that no slip occurs between them. A schematic representation of the physical model and the coordinate system is depicted in Figure 1. The system is considered to be axisymmetric. The thermo-physical properties of the nanoparticles (Oztop and Abu–Nada, 2008) are given in Table I.

Under the above assumptions and following the nanofluid model proposed by Tiwari and Das (2007), with the usual Boussinesq approximation (Schlichting and Gersten, 2001), the governing equations are:

$$\frac{\partial (ru)}{\partial x} + \frac{\partial (rv)}{\partial r} = 0 \tag{1}$$

$$\frac{\partial u}{\partial t'} + u\frac{\partial u}{\partial x} + v\frac{\partial u}{\partial r} = \nu_{nf}\frac{1}{r}\frac{\partial}{\partial r}\left(r\frac{\partial u}{\partial r}\right) + \frac{(\rho\beta)_{nf}}{\rho_{nf}}g(T' - T'_\infty) - \frac{\sigma B_0^2 u}{\rho_{nf}} \tag{2}$$

$$\frac{\partial T'}{\partial t'} + u\frac{\partial T'}{\partial x} + v\frac{\partial T'}{\partial r} = \frac{\kappa_{nf}}{(\rho C_p)_{nf}}\frac{1}{r}\frac{\partial}{\partial r}\left(r\frac{\partial T'}{\partial r}\right) \tag{3}$$

Water and nanoparticles	$\rho(Kg\,m^{-1})$	$C_p(J\,Kg^{-1}\,K^{-1})$	$\kappa(Wm^{-1}\,K^{-1})$	$\beta \times 10^{-5}(K^{-1})$
H_2O	997.1	4179	0.613	21
Al_2O_3	3,970	765	40	0.85
Cu	8,933	385	401	1.67
TiO_2	4,250	686.2	8.9528	0.9
Ag	10,500	235	429	1.89

Table I.
Thermo-physical properties of water and nanoparticles

Equations (1)-(3) are subjected to the following initial and boundary conditions:

$$\begin{aligned} &t' \le 0 : u = 0,\ \ v = 0,\ T' = T'_{\infty} \text{ for all } x \ge 0 \text{ and } r \ge 0 \\ &t' > 0 : u = u_0,\ v = 0,\ T' = T'_{w} \text{ at } r = r_0 \\ &u = 0,\ T' = T'_{\infty} \text{ at } x = 0 \text{ and } r \ge r_0 \\ &u \to 0,\ T' \to T'_{\infty},\ \text{ as } r \to \infty \end{aligned} \tag{4}$$

For nanofluids, the expressions of density ρ_{nf}, thermal expansion coefficient $(\rho\beta)_{nf}$ and heat capacitance $(\rho C_p)_{nf}$ are given by:

$$\begin{aligned} \rho_{nf} &= (1-\phi)\rho_f + \phi\rho_s \\ (\rho\beta)_{nf} &= (1-\phi)(\rho\beta)_f + \phi(\rho\beta)_s \\ (\rho C_p)_{nf} &= (1-\phi)(\rho C_p)_f + \phi(\rho C_p)_s \end{aligned} \tag{5}$$

The effective thermal conductivity of the nanofluid according to the Hamilton and Crosser (1962) model is given by:

$$\frac{\kappa_{eff}}{\kappa_f} = \frac{\kappa_s + (n-1)\kappa_f - (n-1)\phi(\kappa_f - \kappa_s)}{\kappa_s + (n-1)\kappa_f + \phi(\kappa_f - \kappa_s)} \tag{6}$$

where "n" is the empirical shape factor for the nanoparticles. In particular, "n" = 3 for spherical-shaped nanoparticles and "n" = 3/2 for cylindrical ones.

The following dimensionless parameters are defined:

$$\begin{aligned} &X = \frac{x\nu_f}{u_0 r_0^2}, R = \frac{r}{r_0}, U = \frac{u}{u_0}, V = \frac{v r_0}{\nu_f}, t = \frac{t'\nu_f}{r_0^2}, T = \frac{T' - T'_{\infty}}{T'_{w} - T'_{\infty}}, \\ &\Pr = \frac{\nu_f}{\alpha_f}, M = \frac{\sigma B_0^2 r_0^2}{\mu_f}, Gr = \frac{g\beta_f r_0^2 (T'_{w} - T'_{\infty})}{u_0\nu_f} \end{aligned} \tag{7}$$

With the non-dimensional variables in equation (7), equations (1)-(3) become:

$$\frac{\partial(RU)}{\partial X} + \frac{\partial(RV)}{\partial R} = 0 \tag{8}$$

$$\begin{aligned} \frac{\partial U}{\partial t} + U\frac{\partial U}{\partial X} + V\frac{\partial U}{\partial R} = \frac{1}{\left(1-\phi+\phi\frac{\rho_s}{\rho_f}\right)}\Bigg(&\frac{1}{(1-\phi)^{2.5}}\frac{1}{R}\frac{\partial}{\partial R}\left(R\frac{\partial U}{\partial R}\right) \\ &+\left(1-\phi+\phi\frac{(\rho\beta)_s}{(\rho\beta)_f}\right)GrT - MU\Bigg) \end{aligned} \tag{9}$$

$$\frac{\partial T}{\partial t} + U\frac{\partial T}{\partial X} + V\frac{\partial T}{\partial R} = \frac{1}{\left(1-\phi+\phi\frac{(\rho C_p)_s}{(\rho C_p)_f}\right)}\frac{\kappa_{nf}}{\kappa_f}\frac{1}{P_r}\frac{1}{R}\frac{\partial}{\partial R}\left(R\frac{\partial T}{\partial R}\right) \tag{10}$$

The initial and boundary conditions in non-dimensional form are given by:

$$
\begin{aligned}
&t \le 0 : U = 0, V = 0, T = 0 \quad \text{for all } X \text{ and } R \\
&t > 0 : \; U = 1, \; V = 0, \; T = 1 \quad \text{at} \quad R = 1 \\
&U = 0, \; T = 0 \text{ at } X = 0 \\
&U \to 0, \; T \to 0 \text{ as } R \to \infty
\end{aligned}
\tag{11}
$$

3. Numerical solutions to boundary value problem

To solve the unsteady non-linear coupled equations (8)-(10) under the initial and boundary conditions (11), an implicit finite-difference numerical method of the Crank–Nicolson type has been used. The finite difference equations corresponding to equations (8)-(10) are as follows:

$$
\begin{aligned}
&\left[\frac{U_{i,j}^{n+1} - U_{i-1,j}^{n+1} + U_{i,j}^{n} - U_{i-1,j}^{n} + U_{i,j-1}^{n+1} - U_{i-1,j-1}^{n+1} + U_{i,j-1}^{n} - U_{i-1,j-1}^{n}}{4\Delta X}\right] \\
&+\left[\frac{V_{i,j}^{n+1} - V_{i,j-1}^{n+1} + V_{i,j}^{n} - V_{i,j-1}^{n}}{2\Delta R}\right] + \left[\frac{V_{i,j}^{n+1}}{1 + (j-1)\Delta R}\right] = 0
\end{aligned}
\tag{12}
$$

$$
\begin{aligned}
&\left[\frac{U_{i,j}^{n+1} - U_{i,j}^{n}}{\Delta t}\right] + U_{i,j}^{n}\left[\frac{U_{i,j}^{n+1} - U_{i-1,j}^{n+1} + U_{i,j}^{n} - U_{i-1,j}^{n}}{2\Delta X}\right] \\
&+ V_{i,j}^{n}\left[\frac{U_{i,j+1}^{n+1} - U_{i,j-1}^{n+1} + U_{i,j+1}^{n} - U_{i,j-1}^{n}}{4\Delta R}\right] = E_3 \frac{G_r}{2}\left[T_{i,j}^{n+1} + T_{i,j}^{n}\right] \\
&+ E_2\left[\frac{U_{i,j-1}^{n+1} - 2U_{i,j}^{n+1} + U_{i,j+1}^{n+1} + U_{i,j-1}^{n} - 2U_{i,j}^{n} + U_{i,j+1}^{n}}{2(\Delta R)^2}\right] \\
&+ E_2\left[\frac{U_{i,j+1}^{n+1} - U_{i,j-1}^{n+1} + U_{i,j+1}^{n} - U_{i,j-1}^{n}}{4[1 + (j-1)\Delta R]\Delta R}\right] - E_4 \frac{M}{2}\left[U_{i,j}^{n+1} + U_{i,j}^{n}\right]
\end{aligned}
\tag{13}
$$

$$
\begin{aligned}
&\left[\frac{T_{i,j}^{n+1} - T_{i,j}^{n}}{\Delta t}\right] + U_{i,j}^{n}\left[\frac{T_{i,j}^{n+1} - T_{i-1,j}^{n+1} + T_{i,j}^{n} - T_{i-1,j}^{n}}{2\Delta X}\right] + V_{i,j}^{n}\left[\frac{T_{i,j+1}^{n+1} - T_{i,j-1}^{n+1} + T_{i,j+1}^{n} - T_{i,j-1}^{n}}{4\Delta R}\right] \\
&= E_1\left[\frac{T_{i,j-1}^{n+1} - 2T_{i,j}^{n+1} + T_{i,j+1}^{n+1} + T_{i,j-1}^{n} - 2T_{i,j}^{n} + T_{i,j+1}^{n}}{2\mathrm{Pr}\,(\Delta R)^2}\right] \\
&+ E_1\left[\frac{T_{i,j+1}^{n+1} - T_{i,j-1}^{n+1} + T_{i,j+1}^{n} - T_{i,j-1}^{n}}{4\mathrm{Pr}\,[1 + (j-1)\Delta R]\Delta R}\right]
\end{aligned}
\tag{14}
$$

where:

$$E_1 = \frac{\kappa_{nf}}{\kappa_f}\frac{1}{\left(1-\phi+\phi\frac{(\rho C_p)_s}{(\rho C_p)_f}\right)}, E_2 = \frac{1}{(1-\phi)^{2.5}}\frac{1}{\left(1-\phi+\phi\frac{\rho_s}{\rho_f}\right)},$$

$$E_3 = \frac{\left(1-\phi+\phi\frac{(\rho\beta)_s}{(\rho\beta)_f}\right)}{\left(1-\phi+\phi\frac{\rho_s}{\rho_f}\right)}, E_4 = \frac{1}{\left(1-\phi+\phi\frac{\rho_s}{\rho_f}\right)} \quad (15)$$

The region of integration is considered as a rectangle with the sides $X = 0$ to $Xmax = 1$ and $R = 1$ to $Rmax = 16$, where $Rmax$ corresponds to $R \to \infty$ which lies very well outside the momentum and thermal boundary layers. Here the subscripts i and j designate the grid points along the X and R coordinates, respectively, where $X = i\Delta X$ and $R = 1 + j\Delta R$ and the superscript n designates a value of the time t ($= n\Delta t$), with ΔX, ΔR and Δt the mesh sizes in the X, R and t axes, respectively. To obtain an economical and reliable grid system for the computations, a grid independent test has been performed which is shown in Figure 2. The step sizes in X and R directions $\Delta X = 0.02$ and $\Delta R = 0.2$ were found to give accurate results. Also, the time step size dependency has been carried out, from which $\Delta t = 0.01$ was found to give reliable result. During any one-time step, the coefficients $U_{i,j}^n$ and $V_{i,j}^n$ appearing in the difference equations are treated as constants. The values of U, V and T are known at all grid points at $t = 0$ from the initial conditions. The computations of U, V and T at time level (n + 1) using the known values at the previous time level (n) are calculated as follows: the finite-difference equation (14) at every internal nodal point on a particular i-level constitutes a tridiagonal system of equations. Such a system of equations is solved by the Thomas algorithm as described by Carnahan *et al.* (1969). Thus, the values of T are found at every nodal point on a particular i-level at $(n + 1)$th time level. Using the values of T at $(n + 1)$th time level in equation (13), the values of U at $(n + 1)$th time level are found in a similar manner. Thus, the values of T and U are known on a particular i-level. The values of V are calculated explicitly using equation (12) at every nodal point on a particular i-level at $(n + 1)$th time level. This process is repeated for various i-levels. Thus, the values of T, U and V are

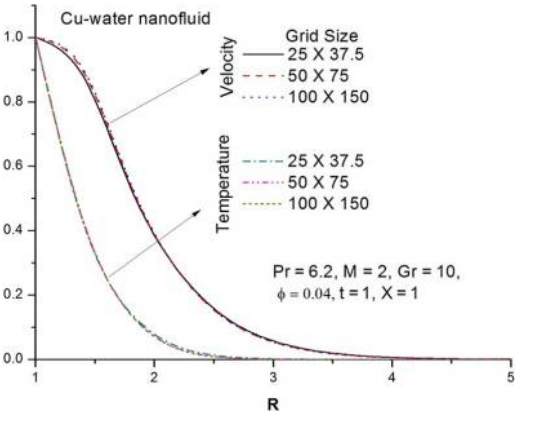

Figure 2.
Grid independent test for velocity and temperature profiles

known at all grid points in the rectangular region at $(n + 1)$th time level. The finite difference scheme is unconditionally stable as discussed by Ganesan and Rani (1998). The truncation error in the finite difference approximation is $O(\Delta t^2+\Delta R^2+\Delta X)$ and it tends to zero as Δt, ΔR and ΔX tend to zero. Therefore, the scheme is compatible. The stability and the compatibility ensure the convergence.

4. Exact solution and validation of the numerical solution

During the initial period, the body forces have not had sufficient time to generate any appreciable motion in the fluid. Hence, both velocity components are negligible for small time t. During this initial transient regime, the heat transfer process is dominated by pure heat conduction. The temperature distribution at early times is, therefore, the same as the transient conduction problem in a semi-infinite solid. The temperature distribution in a semi-infinite solid is given by the following equation (Schlichting and Gersten, 2001; Carslaw and Jaeger, 1959):

$$T' = \left(\frac{r_0}{r}\right)^{1/2} erfc\left(\frac{r - r_0}{2\sqrt{\alpha t'}}\right) \tag{16}$$

with the initial and boundary conditions:

$$\begin{aligned} t' \le 0 &: \; T' = T'_\infty \text{ for all } r \\ t' > 0 &: \; T' = T'_w \text{ at } r = r_0 \end{aligned} \tag{17}$$

By introducing the non-dimensional quantities defined in equation (7), the transient temperature distribution in a semi-infinite solid can be written as:

$$T = R^{-1/2} erfc\left(\frac{R - 1}{2\sqrt{t/\mathrm{Pr}}}\right) \tag{18}$$

with the initial and boundary conditions:

$$\begin{aligned} t \le 0 &: \; T = 0 \text{ for all } R \\ t > 0 &: \; T = 1 \text{ at } R = 1 \end{aligned} \tag{19}$$

The comparison between the transient temperature distributions calculated by equation (18) and by the current implicit finite-difference method (when $\phi = 0$) at two different early times is presented in Figure 3. The plotted results are found to be in excellent agreement and this shows that the current implicit finite-difference method is valid for this type of transient problem.

5. Engineering quantities

In materials processing operations, several physical quantities are of practical interest, for example, the skin-friction coefficient C_f and the local Nusselt number Nu_x, which are defined, respectively, as follows:

$$C_f = \frac{\tau_w}{\rho_f u_0^2}, \; Nu_x = \frac{q_w x}{\kappa_f (T'_w - T'_\infty)} \tag{20}$$

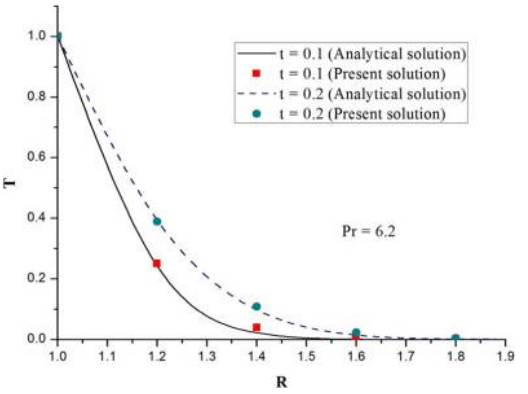

Figure 3.
Comparison of temperature profiles

where τ_w and q_w are the skin-friction coefficient and the rate of heat transfer from the surface of the cylinder, respectively and they are given by:

$$\tau_w = \mu_{nf}\left(\frac{\partial u}{\partial r}\right)_{r=r_0},\ q_w = -\kappa_{nf}\left(\frac{\partial T'}{\partial r}\right)_{r=r_0} \tag{21}$$

Using the non-dimensional variables in equation (7), we get:

$$\mathrm{Re}\ C_f = \frac{1}{(1-\phi)^{2.5}}\left(\frac{\partial U}{\partial R}\right)_{R=1},\ \mathrm{Re}^{-1}Nu_x = -\frac{\kappa_{nf}}{\kappa_f}X\left(\frac{\partial T}{\partial R}\right)_{R=1} \tag{22}$$

where $\mathrm{Re} = \frac{u_0 r_0}{\nu_f}$ is the Reynolds number. The derivatives involved in equation (22) are evaluated by using a *five-point approximation formula*.

6. Results and discussion

To study the behaviour of the transient velocity and temperature *fields*, extensive numerical computations are conducted for various values of the governing thermo-physical parameters and are depicted graphically. We consider a nanofluid containing copper (*Cu*) nanoparticles with water as a base fluid. In this study, we have considered spherical nanoparticles ($n = 3$) with the thermal conductivity (Maxwell Garnett, 1904) and the dynamic viscosity (Brinkman, 1952) shown in Model I in Table II. The Prandtl number *Pr* of the base fluid is kept constant at 6.2. The effects of the magnetic parameter, nanoparticles volume fraction and the thermal Grashof number on the transient velocity and temperature profiles are plotted in the subsequent figures. When $\varphi = 0$, this study reduces the governing equations to those of a regular fluid, i.e. the nanoscale characteristics are eliminated.

The transient velocity profiles of the *Cu*–water nanofluid with the radial coordinate R, at $X = 1.0$, $t = 1$ for different values of the magnetic parameter M, when Pr = 6.2, Gr = 10 and $\phi = 0.04$ are presented in Figure 4. From the figure, it is observed that as the magnetic parameter M increases, the flow rate of the nanofluid retards and thereby gives rise to a decrease in the velocity profiles. The reason behind this phenomenon is that application of a magnetic field to an electrically conducting nanofluid gives rise to a resistive-type force called the Lorentz force. This force has the tendency to slow down the motion of the nanofluid in the boundary layer. Figure 5 depicts the transient velocity

Model	Shape of nanoparticles	Thermal conductivity	Dynamic viscosity
I	Spherical	$\frac{\kappa_{nf}}{\kappa_f} = \frac{\kappa_s + 2\kappa_f - 2\phi(\kappa_f - \kappa_s)}{\kappa_s + 2\kappa_f + \phi(\kappa_f - \kappa_s)}$	$\mu_{nf} = \frac{\mu_f}{(1-\phi)^{2.5}}$
II	Spherical	$\frac{\kappa_{nf}}{\kappa_f} = \frac{\kappa_s + 2\kappa_f - 2\phi(\kappa_f - \kappa_s)}{\kappa_s + 2\kappa_f + \phi(\kappa_f - \kappa_s)}$	$\mu_{nf} = \mu_f(1 + 7.3\,\phi + 123\,\phi^2)$
III	Cylindrical (nanotubes)	$\frac{\kappa_{nf}}{\kappa_f} = \frac{\kappa_s + \frac{1}{2}\kappa_f - \frac{1}{2}\phi(\kappa_f - \kappa_s)}{\kappa_s + \frac{1}{2}\kappa_f + \phi(\kappa_f - \kappa_s)}$	$\mu_{nf} = \frac{\mu_f}{(1-\phi)^{2.5}}$
IV	Cylindrical (nanotubes)	$\frac{\kappa_{nf}}{\kappa_f} = \frac{\kappa_s + \frac{1}{2}\kappa_f - \frac{1}{2}\phi(\kappa_f - \kappa_s)}{\kappa_s + \frac{1}{2}\kappa_f + \phi(\kappa_f - \kappa_s)}$	$\mu_{nf} = \mu_f(1 + 7.3\,\phi + 123\,\phi^2)$

Source: Hamilton and Crosser (1962)

Table II.
Thermal conductivity and dynamic viscosity for various shapes of nanoparticles

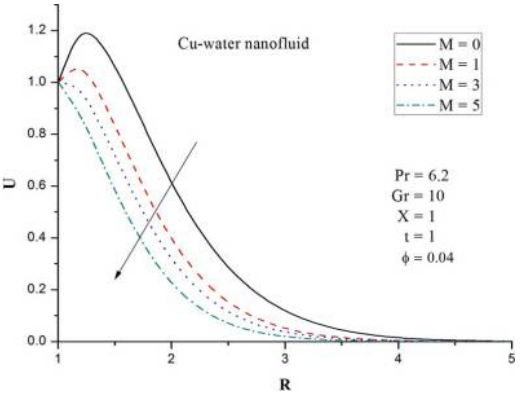

Figure 4.
Effect of magnetic parameter on transient velocity profiles

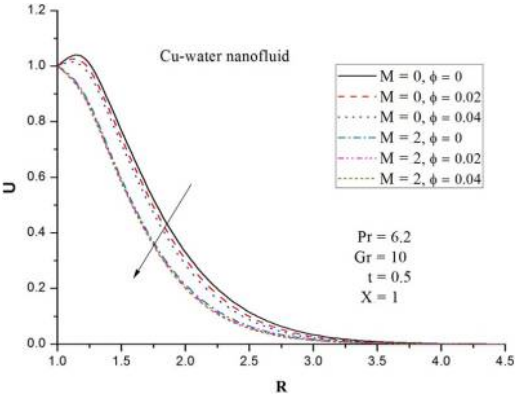

Figure 5.
Effect of nanoparticle volume fraction on transient velocity profiles

profiles of a *Cu*–water nanofluid with the radial coordinate R for different values of the nanoparticles volume fraction ϕ when Pr = 6.2, Gr = 10 at X = 1, t = 0.5 for the cases of both the absence (when M = 0) and the presence (when M = 2) of a magnetic field. From the figure, it is found that, in the absence of a magnetic field (when M = 0), the velocity profiles of a *Cu*–water nanofluid start to increase from the value of unity at the surface of the cylinder, reach their maximum and then monotonically decrease to zero along the radial coordinate R for all values of the nanoparticles volume fraction ϕ. But in the presence of the magnetic field (when M = 2), the velocity profiles of a *Cu*–water nanofluid start to decrease from the value of unity at the surface of the cylinder and then monotonically decrease to zero along the radial coordinate R for all values of nanoparticles volume fraction ϕ. Also, it is found that, in the absence of the magnetic field (when M = 0), the velocity of the nanofluid decreases with an increase in the nanoparticles volume fraction ϕ. In the presence of a magnetic field (when M = 2) also, the similar effect of nanoparticles volume fraction ϕ on the velocity of a *Cu*–water nanofluid is noticed. Furthermore, in the cases of both absence (when M = 0) or presence (when M = 2) of the magnetic field, it is noticed that the velocity of the nanofluid is exceeded by that for pure water (Newtonian viscous fluid).

The effects of the thermal Grashof number Gr on the transient velocity profiles of *Cu*–water nanofluid with the radial coordinate R when Pr = 6.2, M = 2, ϕ = 0.04 at X = 1 and t = 1 are presented in Figure 6. Because the thermal Grashof number Gr signifies the relative effects of the thermal buoyancy force to the viscous hydrodynamic force in the boundary layer region, it is observed from Figure 6 that an increase in Gr leads to an increase in the velocity of the *Cu*–water nanofluid in the boundary layer region. This implies that the thermal buoyancy force tends to accelerate the *Cu*–water nanofluid boundary layer flow. The transient velocity profiles of the *Cu*-water nanofluid with the radial coordinate R for different values of time when Pr = 6.2, M = 2, Gr = 10, ϕ = 0.04 at X = 1 are presented in Figure 7. From the figure, it is observed that the velocity of the *Cu*–water nanofluid is found to increase with increase in time t in the boundary layer region and finally reaches the steady state. The transient temperature profiles of a *Cu*–water nanofluid with the radial coordinate R at X = 1.0, t = 2 for different values of the magnetic parameter M, when Pr = 6.2, Gr = 10 and ϕ = 0.04 are demonstrated in Figure 8. From the figure, it is found that the temperature of the *Cu*–water nanofluid increases with increasing values of M.

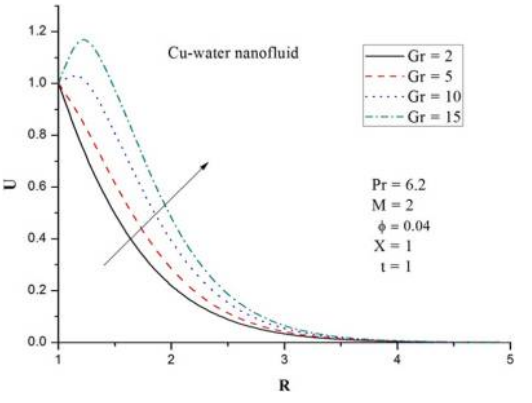

Figure 6.
Effect of thermal Grashof number on transient velocity profiles

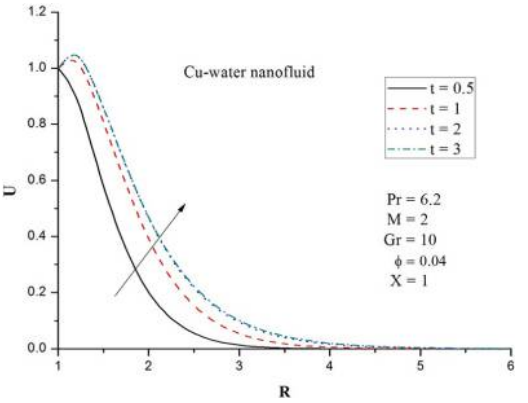

Figure 7.
Effect of time on transient velocity profiles

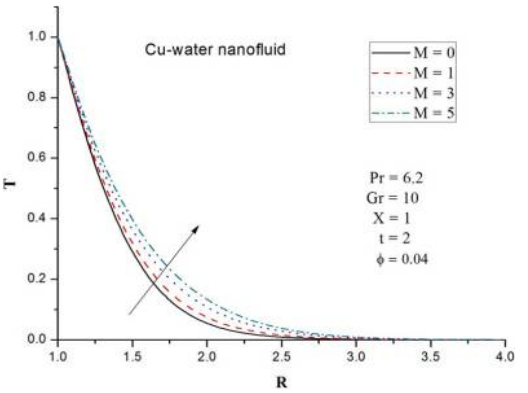

Figure 8.
Effect of magnetic parameter on transient temperature profiles

Figure 9 illustrates the transient temperature profiles of a *Cu*–water nanofluid with the radial coordinate R for different values of the nanoparticles volume fraction ϕ when Pr = 6.2, Gr = 10 at X = 1, t = 2 for the cases of both the presence (when M = 2) and the absence (when M = 0) of the magnetic field. From this figure, the temperature profiles are observed to start with a maximum at the cylinder surface and then monotonically decrease to zero along the radial coordinate R for all values of ϕ. Further, the temperature of the *Cu*–water nanofluid is found to increase with increasing values of ϕ for the cases of both the presence (when M = 2) and the absence (when M = 0) of the magnetic field. Thus, the thermal boundary layer thickness increases with a rise in the values of ϕ in the presence or absence of the magnetic field. The transient temperature profiles of a *Cu*–water nanofluid with the radial coordinate R for various values of the thermal Grashof number Gr when Pr = 6.2, M = 2, ϕ = 0.04 at X = 1 and t = 2 are presented in Figure 10. From this figure, it is observed that an increase in Gr leads to a decrease in the temperature of the *Cu*–water nanofluid in the boundary layer region. The effects of time t on the transient temperature profiles of the *Cu*–water nanofluid with the radial coordinate R when Pr = 6.2, M = 2, Gr = 10, ϕ = 0.04 at X = 1 are presented in Figure 11. From the figure, it is depicted that as time advances, the temperature is found to increase in the boundary layer region and finally reach the steady state.

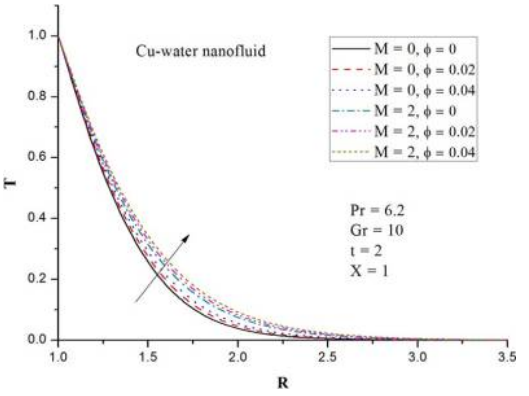

Figure 9.
Effect of nanoparticle volume fraction on transient temperature profiles

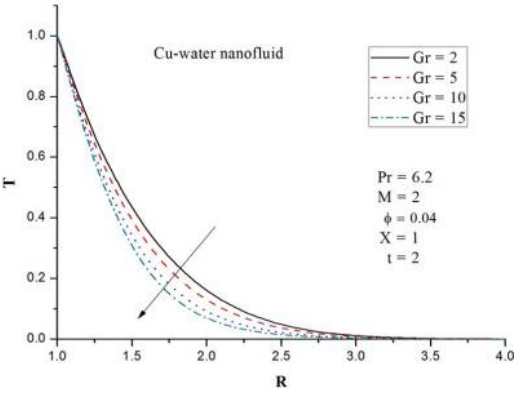

Figure 10.
Effect of thermal Grashof number on transient temperature profiles

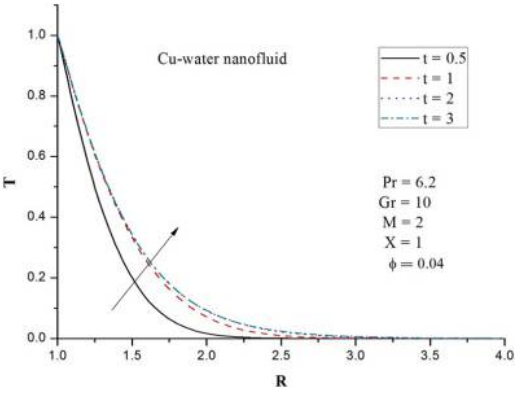

Figure 11.
Effect of time on transient temperature profiles

The numerical values of the local skin-friction coefficient with the axial coordinate X for different values of M, ϕ and Gr are presented in Figures 12-14. From these figures, it is observed that an increase in the values of either M or ϕ, decreases the numerical values of the local skin-friction coefficient, while the opposite effect is observed for *Gr*. It is also observed that the local skin-friction coefficient increases with increasing values of the axial coordinate x for all values of M, ϕ and *Gr*. Furthermore, the skin-friction coefficient of a *Cu*–water nanofluid is less than that of pure water (Newtonian viscous fluid) in the presence (when M = 2) or absence (when M = 0) of a magnetic field.

The axial distributions of the local Nusselt number with different M, ϕ and Gr values are depicted in Figures 15-17. From these figures, the numerical values of the local Nusselt number are found to increase with increasing values of Gr, ϕ and X. But an increase in the values of M reduces the local Nusselt number values. Moreover, the local Nusselt number of a *Cu*–water nanofluid is more than that of a pure water (Newtonian viscous fluid) in the presence (when M = 2) or absence (when M = 0) of a magnetic field. This confirms that the

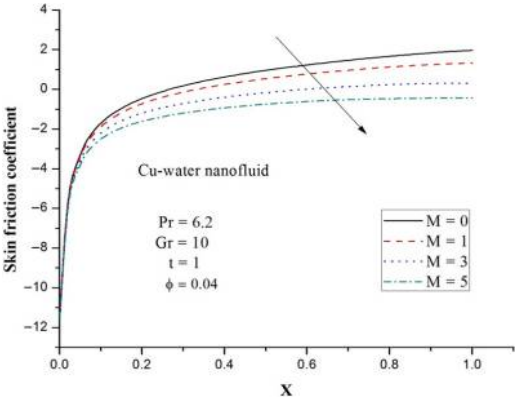

Figure 12.
Effect of magnetic parameter on skin friction coefficient

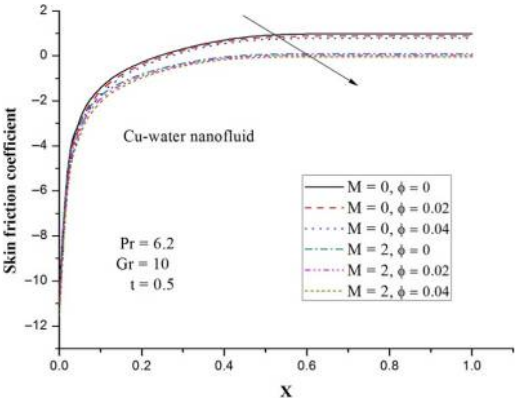

Figure 13.
Effect of nanoparticle volume fraction on skin friction coefficient

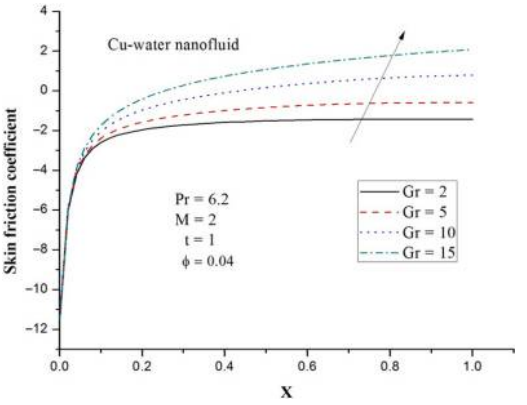

Figure 14.
Effect of thermal Grashof number on skin friction coefficient

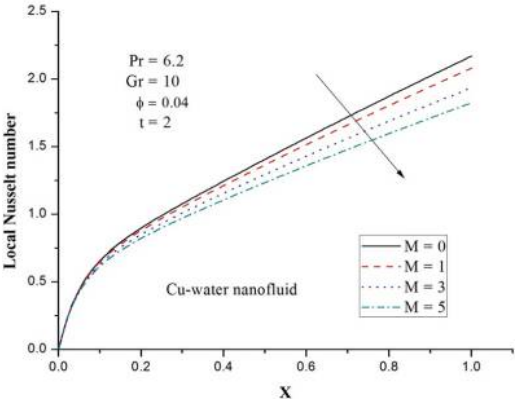

Figure 15.
Effect of magnetic parameter on local Nusselt number

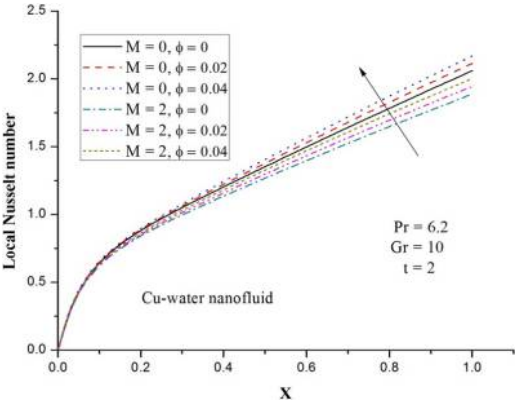

Figure 16.
Effect of nanoparticle volume fraction on local Nusselt number

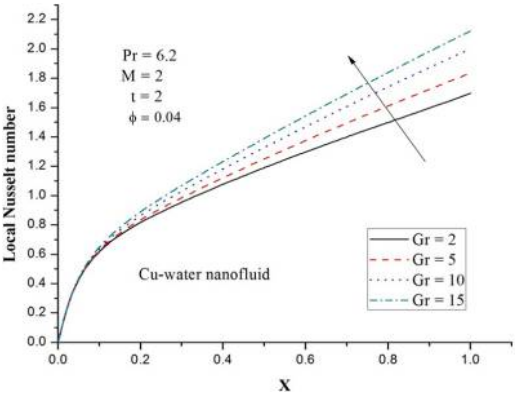

Figure 17.
Effect of thermal Grashof number on local Nusselt number

use of nanofluids is associated with changes in the heat transfer rates which in turn indicate the importance of nanofluids in the cooling and heating processes.

Table III demonstrates the control of nanoparticle volume fraction on the local Nusselt number for various nanofluids, namely, copper–water, aluminium oxide–water, silver–water and titanium oxide–water. It found in Table III that Nusselt number is enhancing with increasing nanoparticle volume fraction. This signifies that greater values of nanoparticle volume fraction tend to improved heat transfer rates. Further the numerical values of Nusselt number are increasing from TiO_2 to Cu through Al_2O_3 and Ag. This indicates that by selecting Cu as a nanoparticle, greater values of Nusselt number can be achieved, while choosing TiO_2 leads to least values of Nusselt number.

7. Conclusions

In this paper, the transient laminar boundary layer free convective flow of nanofluid over a moving vertical cylinder with heat transfer in the presence of applied magnetic field has been investigated. The governing partial differential equations with the corresponding initial and boundary conditions are solved numerically by an implicit finite difference scheme of the Crank–Nicolson type, which is efficient, unconditionally stable and convergent. The effects of the magnetic parameter, thermal Grashof number and the

	Local Nusselt number			
ϕ	C_u	A_g	Al_2O_3	TiO_2
0	1.8872	1.8872	1.8872	1.8872
0.1	2.1813	2.1634	2.1597	2.1054
0.2	2.5094	2.4691	2.4584	2.3391
0.3	2.8926	2.8248	2.7978	2.5965
0.4	3.3631	3.2604	3.2023	2.8914
0.5	3.9743	3.8253	3.7141	3.2459
0.6	4.8266	4.6117	4.4125	3.6973
0.7	6.1403	5.8228	5.4624	4.3119
0.8	8.5317	8.0282	7.2765	5.2215
0.9	14.7506	13.7959	11.2458	6.6942

Table III.
The local Nusselt number for different values of ϕ

nanoparticles volume fraction on the flow and heat transfer characteristics are discussed. The conclusions of the study are as follows:

- An increase in M reduces the velocity and enhances the temperature of a *Cu*–water nanofluid.
- An increase in Gr leads to an increase in the velocity and a decrease in the temperature of a *Cu*–water nanofluid.
- The velocity and temperature of a *Cu*–water nanofluid increase with increasing time.
- The temperature of a *Cu*–water nanofluid increases with a rise in ϕ in the presence or absence of a magnetic field.
- An increase in the values of either M or ϕ, decreases the local skin-friction coefficient, while the opposite effect is observed for *Gr*.
- The local Nusselt number increases with a rise in Gr, ϕ and X values. But an increase in M reduces the local Nusselt number.
- Choosing copper as the nanoparticle type, greater values of Nusselt number can be achieved.

References

Abolbashari, M.H., Freidoonimehr, N., Nazari, F. and Rashidi, M.M. (2014), "Entropy analysis for an unsteady MHD flow past a stretching permeable surface in nano-fluid", *Powder Technology*, Vol. 267, pp. 256-267.

Brinkman, H.C. (1952), "The viscosity of concentrated suspensions and solution", *The Journal of Chemical Physics*, Vol. 20, pp. 571-581.

Carnahan, B., Luther, H.A. and Wilkes, J.O. (1969), *Applied Numerical Methods*, John Wiley & Sons, New York, NY.

Carslaw, H.S. and Jaeger, J.C. (1959), *Conduction of Heat in Solids*, Oxford University Press, London.

Chen, T.S. and Yuh, C.F. (1980), "Combined heat and mass transfer in natural convection along a vertical cylinder", *International Journal of Heat and Mass Transfer*, Vol. 23, pp. 451-461.

Ganesan, P. and Rani, H.P. (1998), "Transient natural convection along vertical cylinder with heat and mass transfer", *Heat and Mass Transfer*, Vol. 33, pp. 449-455.

Ganesan, P. and Rani, H.P. (1999), "Unsteady free convection on a vertical cylinder with variable heat and mass flux", *Heat and Mass Transfer*, Vol. 35, pp. 259-265.

Hamilton, R.L. and Crosser, O.K. (1962), "Thermal conductivity of heterogeneous two component system", *Industrial and Engineering Chemistry Fundamentals*, pp. 187-191.

Khedr, M.E., Chamkha, A.J. and Bayomi, M. (2009), "MHD flow of a micropolar fluid past a stretched permeable surface with heat generation or absorption", *Nonlinear Analysis: Modelling and Control*, Vol. 14, pp. 27-40.

Lee, H.R., Chen, T.S. and Armaly, B.F. (1988), "Natural convection along slender vertical cylinders with variable surface temperature", *Journal of Heat Transfer*, Vol. 100, pp. 103-108.

Loganathan, P., Nirmal Chand, P. and Ganesan, P. (2013), "Radiation effects on an unsteady natural convective flow of a nanofluid past an infinite vertical plate", *NANO: Brief Reports and Reviews*, Vol. 8 No. 1, pp. 1-10.

Maxwell Garnett, J.C. (1904), "Colours in metal glasses and in metallic films", *Philosophical Transactions of the Royal Society A*, Vol. 203, pp. 385-420.

Nandkeolyar, R., Seth, G.S., Makinde, O.D., Sibanda, P. and Ansari, M.S. (2013), "Unsteady hydromagnetic natural convection flow of a dusty fluid past an impulsively moving vertical plate with ramped temperature in the presence of thermal radiation", *ASME Journal of Applied Mechanics*, Vol. 80 No. 6, pp. 1-9, doi: 10.1115/1.4023959.

Oztop, H.F. and Abu–Nada, E. (2008), "Numerical study of natural convection in partially heated rectangular enclosures filled with nanofluids", *International Journal of Heat Fluid Flow*, Vol. 29, pp. 1326-1336.

Rajesh, V. and Anwar Beg, O. (2014), "MHD transient nanofluid flow and heat transfer from a moving vertical cylinder with temperature oscillation", *Computational Thermal Sciences*, Vol. 6 No. 5, pp. 439-450.

Rajesh, V., Anwar Beg, O. and Mallesh, M.P. (2016a), "Transient nanofluid flow and heat transfer from a moving vertical cylinder in the presence of thermal radiation: Numerical study", *Proceedings of the Institution of Mechanical Engineers, Part N: Journal of Nanoengineering and Nanosystems*, Vol. 230 No. 1, pp. 3-16.

Rajesh, V., Mallesh, M.P. and Sridevi, C. (2015a), "Transient MHD nanofluid flow and heat transfer due to a moving vertical plate with thermal radiation and temperature oscillation effects", *Procedia Engineering*, Vol. 127, pp. 901-908.

Rajesh, V., Chamkha, A.J. and Mallesh, M.P. (2016b), "Transient MHD free convection flow and heat transfer of nanofluid past an impulsively started semi-infinite vertical plate", *Journal of Applied Fluid Mechanics*, Vol. 9.

Rajesh, V., Chamkha, A.J. and Mallesh, M.P. (2016c), "Nanofluid flow past an impulsively started vertical plate with variable surface temperature", *International Journal of Numerical Methods for Heat & Fluid Flow*, Vol. 26 No. 1, pp. 1-21.

Rajesh, V., Mallesh, M.P. and Anwar Bég, O. (2015b), "Transient MHD free convection flow and heat transfer of nanofluid past an impulsively started vertical porous plate in the presence of viscous dissipation", *Procedia Material Science*, Vol. 80, pp. 10-89.

Rani, H.P. (2003), "Transient natural convection along a vertical cylinder with variable surface temperature and mass diffusion", *Heat Mass Transfer*, Vol. 40, pp. 67-73.

Rashidi, M.M., Momoniat, E. and Rostami, B. (2012), "Analytic approximate solutions for MHD boundary-layer viscoelastic fluid flow over continuously moving stretching surface by homotopy analysis method with two auxiliary parameters", *Journal of Applied Mathematics*, Vol. 2012, pp. 1-19.

Rashidi, M.M. and Erfani, E. (2012), "Analytical method for solving steady MHD convective and slip flow due to a rotating disk with viscous dissipation and Ohmic heating", *Engineering Computations: International Journal for Computer-Aided Engineering and Software*, Vol. 29 No. 6, pp. 562-579.

Rashidi, M.M., Ali, M., Freidoonimehr, N., Rostami, B. and Anwar Hossain, M. (2014), "Mixed convective heat transfer for MHD viscoelastic fluid flow over a porous wedge with thermal radiation", *Advances in Mechanical Engineering*, Vol. 2014, pp. 1-10.

Schlichting, H. and Gersten, K. (2001), *Boundary Layer Theory*, Springer-Verlag, New York, NY.

Seth, G.S. and Sarkar, S. (2015), "MHD natural convection heat and mass transfer flow past a time dependent moving vertical plate with ramped temperature in a rotating medium with hall effects, radiation and chemical reaction", *Journal of Mechanics*, Vol. 31 No. 1, pp. 91-104.

Seth, G.S., Sarkar, S. and Nandkeolyar, R. (2015b), "Unsteady hydromagnetic natural convection flow past an impulsively moving vertical plate with Newtonian heating in a rotating system", *Journal of Applied Fluid Mechanics*, Vol. 8 No. 3, pp. 623-633.

Seth, G.S. and Ansari, M.S. (2010), "MHD natural convection flow past an impulsively moving vertical plate with ramped wall temperature in the presence of thermal diffusion with heat absorption", *International Journal of Applied Mechanics and Engineering*, Vol. 15 No. 1, pp. 199-215.

Seth, G.S., Sarkar, S., Hussain, S.M. and Mahato, G.K. (2015a), "Effects of hall current and rotation on hydromagnetic natural convection flow with heat and mass transfer of a heat absorbing fluid past an impulsively moving vertical plate with ramped temperature", *Journal of Applied Fluid Mechanics*, Vol. 8 No. 1, pp. 159-171.

Seth, G.S., Ansari, M.S. and Nandkeolyar, R. (2011a), "MHD natural convection flow with radiative heat transfer past an impulsively moving plate with ramped wall temperature", *Heat and Mass Transfer*, Vol. 47 No. 5, pp. 551-561.

Seth, G.S., Nandkeolyar, R. and Ansari, M.S. (2011b), "Effect of rotation on unsteady hydromagnetic natural convection flow past an impulsively moving vertical plate with ramped temperature in a porous medium with thermal diffusion and heat absorption", *International Journal of Applied Mathematics and Mechanics*, Vol. 7 No. 21, pp. 52-69.

Seth, G.S., Nandkeolyar, R. and Ansari, M.S. (2013), "Effects of thermal radiation and rotation on unsteady hydromagnetic free convection flow past an impulsively moving vertical plate with ramped temperature in a porous medium", *Journal of Applied Fluid Mechanics*, Vol. 6 No. 1, pp. 27-38.

Sparrow, E.M. and Gregg, J.L. (1956), "Laminar free convection heat transfer from the outer surface of a vertical circular cylinder", *Trans ASME*, Vol. 78, pp. 1823-1830.

Tiwari, R.K. and Das, M.K. (2007), "Heat transfer augmentation in a two-sided lid-driven differentially heated square cavity utilizing nanofluids", *International Journal of Heat and Mass Transfer*, Vol. 50, pp. 9-10.

Velusamy, K. and Garg, V.K. (1992), "Transient natural convection over a heat generating vertical cylinder", *International Journal of Heat and Mass Transfer*, Vol. 35, pp. 1293-1306.

Corresponding author
V. Rajesh can be contacted at: v.rajesh.30@gmail.com